Article

Synthesis, Structure, and Luminescence of a Molecular Europium Tetracyanoplatinate Incorporating 4,5-Diazafluoren-9-One

Richard E. Sykora

Department of Chemistry, University of South Alabama, 6040 USA Drive South, Chemistry Building Room 223, Mobile, AL 36688, USA; rsykora@southalabama.edu; Tel.: +1-(251)-460-7422

Abstract: $Eu_2(Pt(CN)_4)_3(H_2O)_{12}\cdot 4C_{11}H_6N_2O\cdot 6H_2O$ represents a new member to the lanthanide tetracyanoplatinate family of materials. The synthesis, single-crystal X-ray structure, and photoluminescence properties of this compound are reported herein. The compound contains dimeric $[Eu_2(Pt(CN)_4)_3(H_2O)_{12}]$ molecules in which the Eu^{3+} sites are connected with trans-bridging $[Pt(CN)4]^{2-}$ anions and co-crystallized along with 4,5-diazafluoren-9-one (dafone) and lattice water. Prominent noncovalent interactions that stabilize the structure include H-bonding as well as short stacking interactions involving the planar tetracyanoplatinate anions in conjunction with the planar dafone molecules. Photoluminescence measurements illustrate that $Eu_2(Pt(CN)_4)_3(H_2O)_{12}\cdot 4C_{11}H_6N_2O\cdot 6H_2O$ contains multiple emitting states and also displays enhanced Eu^{3+}-based emission due to energy transfer within the compound.

Keywords: europium; tetracyanoplatinate; 4,5-diazafluoren-9-one; single-crystal X-ray diffraction; photoluminescence

1. Introduction

Cyanide-bridged, bimetallic compounds exhibit interesting structural and material properties, which have provided the basis for exploration of this research area [1–4]. Magnetic applications have dominated the work centering around transition-metal hexacyanides or Prussian blue type compounds [5–7], while optical applications have been the main research focus regarding the dicyanometallates of Au and Ag and the tetracyanometallates of Pd and Pt [8–10]. However, a multitude of research reports on the rare-earth cyanometallates focusing on the synthetic, structural, spectroscopic, and catalytic aspects of these materials are also available in the literature [11–15]. In many such compounds, metallophilic interactions are recognized as a major force determining structural dimensionality and properties [16,17]. For example, the square-planar $[Pt(CN)_4]^{2-}$ anions readily associate into 1-D chains [18], or smaller geometric units [19], containing short Pt–Pt interactions and are prominent in the families of tetracyanoplatinate compounds.

Lanthanide ion luminescence is ideal for a number of applications, e.g., fluoroimmunoassays, [20,21] cellular imaging [22,23], and optical communications [24,25], due to its sharp *f-f* transitions and high color purity. However, because direct absorption of the *f-f* excited states is very inefficient, optimizing chromophoric ligands to enhance lanthanide-ion luminescence has been and continues to be an active area for researchers. Many organic [26,27] and inorganic [28,29] donors have been investigated over the years to efficiently transfer energy to acceptor lanthanide ions, including the aforementioned cyanometallate systems.

Cooperative enhancement of Ln^{3+} emissions by utilizing multiple donors has received more attention recently [30–32]. Efforts have primarily focused on preparing Ln^{3+} compounds that contain multiple light-harvesting moieties; for example, compounds containing multiple organic chromophores such as $Ln(tfnb)_3$dafone (Htfnb = 1-(2-naphthyl)-

4,4,4-trifluoro-1,3-butanedionate; dafone = 4,5-diazafluoren-9-one) have been previously reported [30]. Our group has worked on preparing mixed ligand systems incorporating combinations of purely inorganic and inorganic/organic ligands [31–35]. Cyanometallate systems involving both linear d^{10} and square planar d^8 cyanometallates and/or cyclic amines such as 2,2′-bipyridine (bpy) [33], 1,10-phenanthroline (phen) [34], or 2,2′:6′,2″-terpyridine [31,32,34] have been reported. In compounds such as $Eu(C_{15}H_{11}N_3)(H_2O)_2$ $(NO_3)(Pt(CN)_4)\cdot CH_3CN$ [31,32] and $K_2[Tb(H_2O)_4(Pt(CN)_4)_2]Au(CN)_2\cdot 2H_2O$ [33], where both donor groups have a direct pathway to a given Ln^{3+} cation, the emission from the Ln^{3+} has been shown to be enhanced relative to direct Ln^{3+} excitation via energy transfer by exciting either donor ligand. Continuing with this area of research, herein we report on a novel, molecular europium tetracyanoplatinate compound that incorporates both tetracyanoplatinate and 4,5-diazafluoren-9-one (dafone), $[Eu_2(Pt(CN)_4)_3(H_2O)_{12}]\cdot 4C_{11}H_6N_2O\cdot 6H_2O$.

2. Materials and Methods

$Eu(NO_3)_3\cdot 6H_2O$ (Strem, 99.9%), 4,5-diazafluoren-9-one (Alfa Aesar, 97%), and $K_2Pt(CN)_4$ $\cdot 3H_2O$ (Alfa Aesar, 99.9%) were used as received without further purification. The reactions reported produced the highest observed yields of the respective compounds. IR spectra were obtained on room-temperature samples pressed into KBr pellets using a ThermoScientific Nicolet iS50 FT-IR (Thermo Fisher Scientific, Madison, WI, USA) over the range of 400 to 4000 cm^{-1}.

2.1. The Synthesis of [Eu₂(Pt(CN)₄)₃(H₂O)₁₂]·4C₁₁H₆N₂O·6H₂O (C₁₁H₆N₂O = 4,5-Diazafluoren-9-One)

The synthesis of the title compound was carried out by mixing 1 mL of a 0.05 M solution of the appropriate lanthanide nitrate in THF, 1 mL of 0.05 M $K_2[Pt(CN)_4]$ (aq), and 1 mL of 0.10 M 4,5-diazafluoren-9-one in THF. Slow evaporation of the solvent over a period of several days resulted in the crystallization of colorless needles with a yield of 87%. Elemental analysis: Calculated for $C_{56}H_{60}Eu_2N_{20}O_{22}Pt_3$: C, 29.8%; H, 2.68%; N, 12.4%. Found: C, 27.8%, H, 1.64%, N, 12.6%. Challenges associated with CHN analyses in organometallic compounds have been discussed previously [36,37]. IR (KBr, cm^{-1}): 3432 (s, br), 2165 (m), 2151 (s), 2130 (s), 1734 (s), 1669 (m, br), 1624 (m, br), 1596 (s), 1565 (s), 1470 (w), 1406 (s), 1384 (m), 1266 (m), 1161 (w), 1102 (m), 1087 (w), 1034 (w), 923 (m), 759 (s), 728 (w), 636 (w), 500 (w), 478 (w), 456 (w), 436 (w), 428 (w).

2.2. Single-Crystal X-ray Diffraction Studies

Single crystals of the title compound were selected, mounted on quartz fibers, and aligned with a digital camera on an Oxford Xcalibur E single-crystal X-ray diffractometer. Intensity measurements were performed using Mo Kα radiation from a sealed-tube Enhance X-ray source and an Eos area detector. CrysAlisPro [38] was used for the preliminary determination of the cell constants, for the data collection strategy, and for the data collection control. Following data collection, CrysAlisPro was also used to integrate the reflection intensities, apply an absorption correction to the data, and perform a global cell refinement.

For all structure analyses, the program suite SHELX (v. 2014/3) was used for the structure solution (XS) and least-squares refinement (XL) [39]. The initial structure solutions were carried out using direct methods, and the remaining atomic positions were located in difference maps. The final refinements included anisotropic displacement parameters for all non-hydrogen atoms. Some crystallographic details are listed in Table 1, and additional details are available as Supplementary Materials. CCDC 2169999 contains the supplementary crystallographic data for this paper. These data can be obtained free of charge via http://www.ccdc.cam.ac.uk/conts/retrieving.html (accessed on 29 August 2022, or from the CCDC, 12 Union Road, Cambridge CB2 1EZ, UK; Fax: +44 1223 336033; E-mail: deposit@ccdc.cam.ac.uk)

Table 1. Crystallographic data for $[Eu_2(Pt(CN)_4)_3(H_2O)_{12}] \cdot 4C_{11}H_6N_2O \cdot 6H_2O$.

Formula	$C_{56}H_{60}Eu_2N_{20}O_{22}Pt_3$
Formula weight (amu)	2254.43
Crystal System	Monoclinic
space group	$P2_1/n$
a (Å)	10.9678(3)
b (Å)	25.1612(6)
c (Å)	13.3381(3)
β (deg)	91.400(2)
V (Å^3)	3679.72(16)
Z	2
T (K)	290
λ (Å)	0.71073
ρ_{calcd} (g cm^{-3})	2.035
μ(Mo $K\alpha$) (mm^{-1})	7.446
$R(F_o)$ for $F_o^2 > 2\sigma(F_o^2)$ [a]	0.0261
$R_w(F_o^2)$ [b]	0.0476

[a.] $R(F_o) = \sum ||F_o| - |F_c|| / \sum |F_o|$. [b.] $R_w(F_o^2) = \left[\sum \left[w(F_o^2 - F_c^2)^2 \right] / \sum w F_o^4 \right]^{1/2}$.

2.3. Photoluminescence Studies

The luminescence measurements were conducted utilizing a Photon Technology International (PTI) spectrometer system. This instrument utilizes a 75 W Xe source and PMT detectors (Hamamatsu model 928 tube) operating in digital (photon counting) mode to measure steady-state emission and excitation spectra. Time-dependent measurements were performed by utilizing a variable, pulsed Xe source and gated photomultiplier tubes (Hamamatsu model 928 tube). The selection of excitation and emission wavelengths were conducted by means of computer-controlled, autocalibrated "QuadraScopic" monochromators, which are equipped with aberration-corrected emission and excitation optics. The emission monochromators were calibrated, using a NIST traceable tungsten light, to compensate for the wavelength-dependent variation in the system on the emission channel. The instrument operation, data collection, and handling were all controlled using the FeliX32 fluorescence spectroscopic package. All of the spectroscopic experiments are conducted on neat crystalline samples, individually screened for phase purity using single-crystal X-ray diffraction and held in sealed quartz capillary tubes.

3. Results and Discussion

3.1. Structural Studies

The structure of the europium complex in $[Eu_2(Pt(CN)_4)_3(H_2O)_{12}] \cdot 4C_{11}H_6N_2O \cdot 6H_2O$ is molecular, and contains a dimeric core with the two Eu(III) sites joined by a trans-bridging $Pt(CN)_4^{2-}$ anion. A thermal ellipsoid plot of the asymmetric unit with the included atomic labeling scheme is illustrated in Figure 1, and the dimer is illustrated in Figure 2. This dimeric core is reminiscent of that contained in $[\{Eu(DMSO)_2(C_{12}H_8N_2)(H_2O)_3\}_2Pt(CN)_4]^{2+}$ complex cations [40]. The slightly distorted, square-antiprismatic coordination geometry around each Eu(III) center results from one monodentate N-bound $Pt(CN)_4^{2-}$ anion, one trans-bridging N-bound $Pt(CN)_4^{2-}$ anion, and six water molecules. Pt1, occupying the trans-bridging $Pt(CN)_4^{2-}$, resides on an inversion center, which relates the two halves of the dimeric complex cation by symmetry.
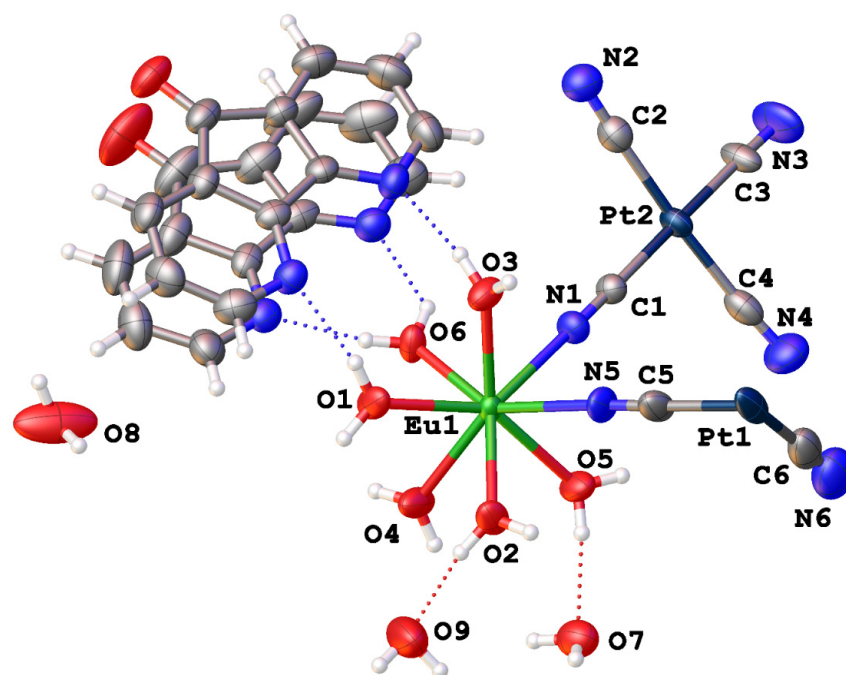
Figure 1. A thermal ellipsoid plot (50%) shows the asymmetric unit of the title compound. The Eu and Pt sites contain square-antiprismatic and square-planar coordination environments, respectively. Pt1 is located on an inversion center. The atoms in the dafone molecules are not labeled for clarity.
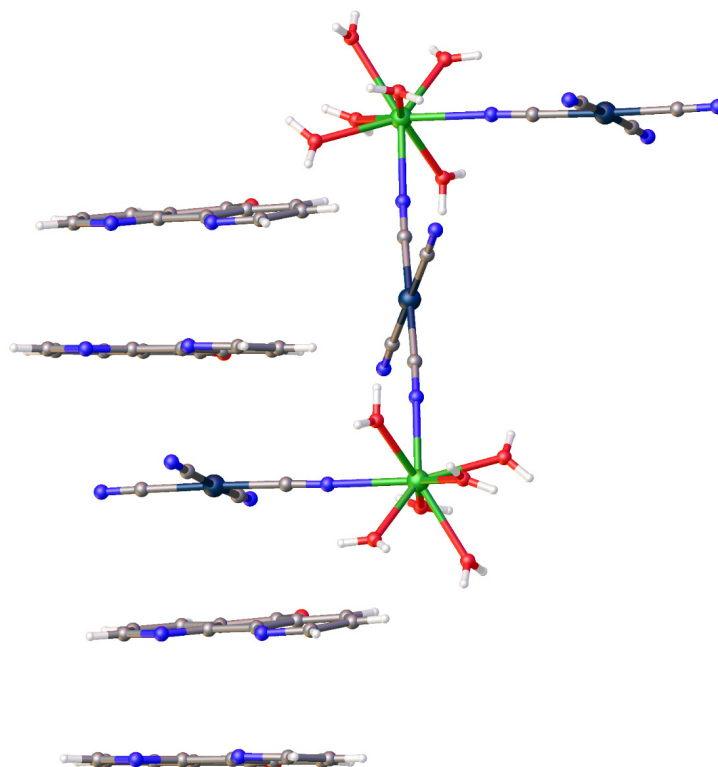

Figure 2. A ball and stick plot illustrating the molecular dimer with the central trans-bridging tetracyanoplatinate anion. The stacking of the dafone and tetracyanoplatinate anions is also shown.

In addition to the metal-centered complexes, dafone molecules and waters of hydration are co-crystallized within the lattice and add to its structural stability with many and varied H-bonding and pi-stacking interactions. The number of H-bonds for the complex waters is maximized via the formation of two H-bond donor interactions, as described

in detail in Table 2. All of the following acceptors are involved in at least one H-bonding interaction in the structure: uncoordinated N-terminated cyanide, lattice water, dafone-N, or dafone-O. Furthermore, every non-coordinated cyanide from each tetracyanoplatinate anion is involved in an H-bonding acceptor interaction with an O−H donor from either a coordinated or uncoordinated water molecule. In addition to these common types of van der Waals interactions mentioned above, $[Eu_2(Pt(CN)_4)_3(H_2O)_{12}]\cdot4C_{11}H_6N_2O\cdot6H_2O$ contains additional intermolecular interactions as shown in Figure 2. The structure contains stacks of alternating pairs of dafone molecules and tetracyanoplatinate anions. The pi-stacking distances between dafone molecules are ~3.42 Å, and the plane-centroid distances between dafone and tetracyanoplatinate are ~3.55 Å within these 1-D stacks. Previous structural studies containing square planar Pt(II) and organic aromatics have described similar interactions [41]. The structure of $[Eu_2(Pt(CN)_4)_3(H_2O)_{12}]\cdot4C_{11}H_6N_2O\cdot6H_2O$ does not contain metallophilic (Pt—Pt) interactions which are present in many structures containing tetracyanoplatinate [18].

Table 2. Hydrogen-bond geometries (Å, º) for $[Eu_2(Pt(CN)_4)_3(H_2O)_{12}]\cdot4C_{11}H_6N_2O\cdot6H_2O$.

D–H···A	D–H	H···A	D···A	D–H···A
O(1)–H(1A)···N(3 [i])	0.85	1.88	2.700(6)	160.5
O(1)–H(1B)···N(10)	0.85	2.06	2.893(5)	168.7
O2–H2A···O11 [ii]	0.85	2.14	2.898(5)	148.1
O2–H2B···O9	0.85	1.81	2.635(5)	165.0
O3–H3A···N9	0.85	1.90	2.735(5)	165.5
O3–H3B···O8 [iii]	0.85	1.86	2.714(5)	179.3
O4–H4A···N2 [iv]	0.85	2.06	2.881(6)	161.3
O4–H4B···O7	0.85	3.10	3.798(5)	140.8
O5–H5A···O7	0.85	1.91	2.740(5)	166.1
O5–H5B···O7 [v]	0.85	1.95	2.795(5)	169.9
O6–H6A···N7	0.85	2.15	2.807(5)	134.3
O6–H6B···N8	0.85	1.87	2.703(5)	165.5
O9–H9A···N4 [v]	0.85	2.03	2.884(7)	178.9

Symmetry transformation used to generate equivalent atoms: (i) x, y, z + 1; (ii) −x + ½, y − ½, −z + ½; (iii) x + ½, −y + ½, z − ½; (iv) x − ½, −y + ½, z + ½; (v) −x, −y, −z.

Select bond distances for $[Eu_2(Pt(CN)_4)_3(H_2O)_{12}]\cdot4C_{11}H_6N_2O\cdot6H_2O$ can be found in Table 3. A clear trend in the Eu−O and Eu−N distances among the various coordinating ligands is observed; Eu−N(TCP) distances are longer (average of 2.507 Å) by over a tenth of an Angstrom relative to the Eu−O(H$_2$O) distances (average of 2.393 Å). The Pt−C distances vary little, ranging from 1.989(5) to 2.034(8) Å with an average value of 2.003 Å, with no clear trend in bridging versus terminal groups. All of these bond distances are within normal ranges as found in previously reported Eu(III) tetracyanoplatinate structures [31,32,35].

Table 3. Selected Bond Distances (Å) for $[Eu_2(Pt(CN)_4)_3(H_2O)_{12}]\cdot4C_{11}H_6N_2O\cdot6H_2O$.

Distances (Å)			
Eu1–N1	2.513 (4)	Pt1–C5	1.989 (5)
Eu1–N5	2.501 (4)	Pt1–C6	2.034 (8)
Eu1–O1	2.386 (3)	Pt1−C5 [i]	1.989 (5)
Eu1–O2	2.411 (3)	Pt1−C6 [i]	2.034 (8)
Eu1–O3	2.373 (3)	Pt2–C1	1.989 (5)
Eu1–O4	2.456 (3)	Pt2–C2	1.989 (6)
Eu1–O5	2.397 (3)	Pt2–C3	2.007 (5)
Eu1–O6	2.335 (3)	Pt2–C4	1.994 (6)

Symmetry transformation used to generate equivalent atoms: (i) −x + 1, −y, −z.

3.2. Photoluminescence Studies

The solid-state emission spectra of $[Eu_2(Pt(CN)_4)_3(H_2O)_{12}]\cdot 4C_{11}H_6N_2O\cdot 6H_2O$ are shown in Figure 3, and band locations and assignments are given in Table 4. These data illustrate that $[Eu_2(Pt(CN)_4)_3(H_2O)_{12}]\cdot 4C_{11}H_6N_2O\cdot 6H_2O$ displays a number of sharp emission bands, some strong, stretching across the visible region, in addition to a weak, broad emission band centered at approximately 510 nm. The assignment of the sharp emission bands in the spectrum is straightforward as these originate from $f-f$ emissions of two different Eu(III) excited states. Expectedly, direct Eu(III) excitation, e.g., the $^5D_2 \leftarrow ^7F_0$ transition at 467 nm, provides relatively weak Eu-based emission due to low absorption of the f-element ion, however, excitation with higher energy UV radiation in the range of 270 to 450 nm leads to similar emission profiles with much greater intensities.
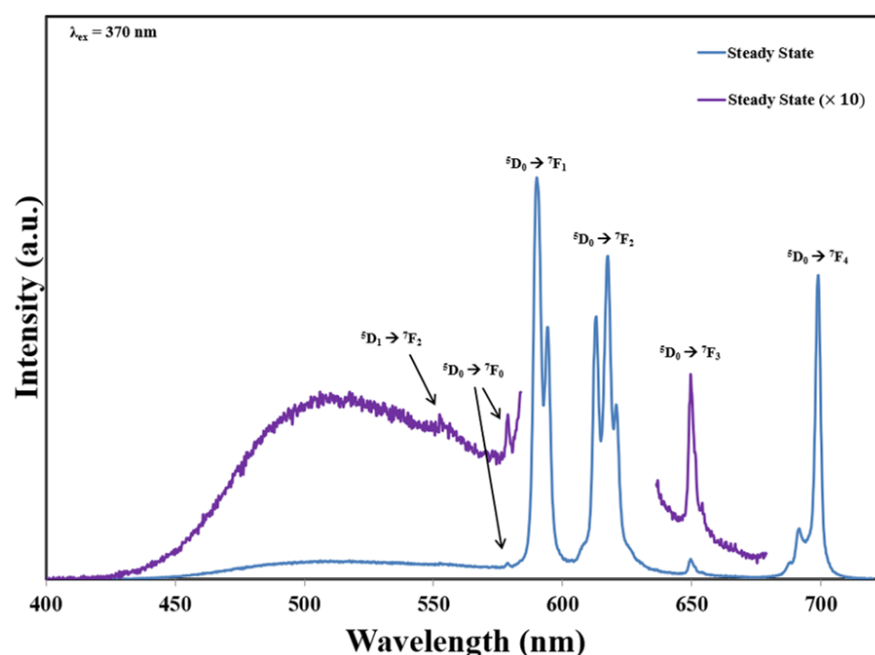

Figure 3. Room temperature, solid-state emission spectra collected with 370 nm excitation.

Table 4. Band locations (most intense) and assignments for the emission transitions of $[Eu_2(Pt(CN)_4)_3(H_2O)_{12}]\cdot 4C_{11}H_6N_2O\cdot 6H_2O$.

Assignment	λ (nm)
$^5D_1 \rightarrow ^7F_2$	552
$^5D_0 \rightarrow ^7F_0$	579
$^5D_0 \rightarrow ^7F_1$	590
$^5D_0 \rightarrow ^7F_2$	617.5
$^5D_0 \rightarrow ^7F_3$	649.5
$^5D_0 \rightarrow ^7F_4$	699

The $^5D_0 \rightarrow ^7F_0$ transition, oftentimes just referred to as the $0-0$ transition, is observed at 579 nm and signifies a strong electric dipole contribution. The observance of this $0-0$ transition with only a single band is in line with the crystallographic structure analysis that shows a C_1 site symmetry for the single Eu(III) site in the compound. The breaking of the degeneracy of the $^5D_0 \rightarrow ^7F_1$ transition resulting in the observance of multiple Stark components is also consistent with a low site symmetry for Eu(III) (C_1 symmetry) [42]. The $^5D_0 \rightarrow ^7F_2$ transition shows splitting into five Stark components even at room temperature. Although the two outer bands are not completely resolved, this splitting is estimated at 100 cm^{-1}. The Eu^{3+} ion emission has a lifetime of 120 µs, measured for the $^5D_0 \rightarrow ^7F_1$ transition, in the title compound. While this value is in line with the reported Eu^{3+} lifetimes

in other systems, the differences can be attributed to the number of H_2O molecules directly coordinated to the Eu(III) ion in the different compounds [43] or to the relative amount of hydrogen bonding involved in systems containing charge transfer interactions with Eu(III) acceptors [44].

The assignment of the broad emission band centered at approximately 510 nm is not as straightforward. Performing time-delay emission experiments, with pulsed excitation, reveals that the lifetime of this emission is much shorter than the Eu^{3+} *f-f* emission bands. Figure 4 shows the decoupled emission from the title compound at different time delays. This indicates that the emission originates from different emitting species within the compound. Since dafone and tetracyanoplatinate can both independently present broad emission bands within this spectral region [30,31], the emission spectra alone is inconclusive. However, the excitation spectra shown in Figure 5 are not reminiscent of the absorption features of either dafone or tetracyanoplatinate alone. Further, the similarity of the excitation bands upon monitoring the Eu(III) emission or the ligand-based emission band is direct evidence for the existence of energy transfer in the system. All of this together indicates the existence of exciplex formation within this compound.
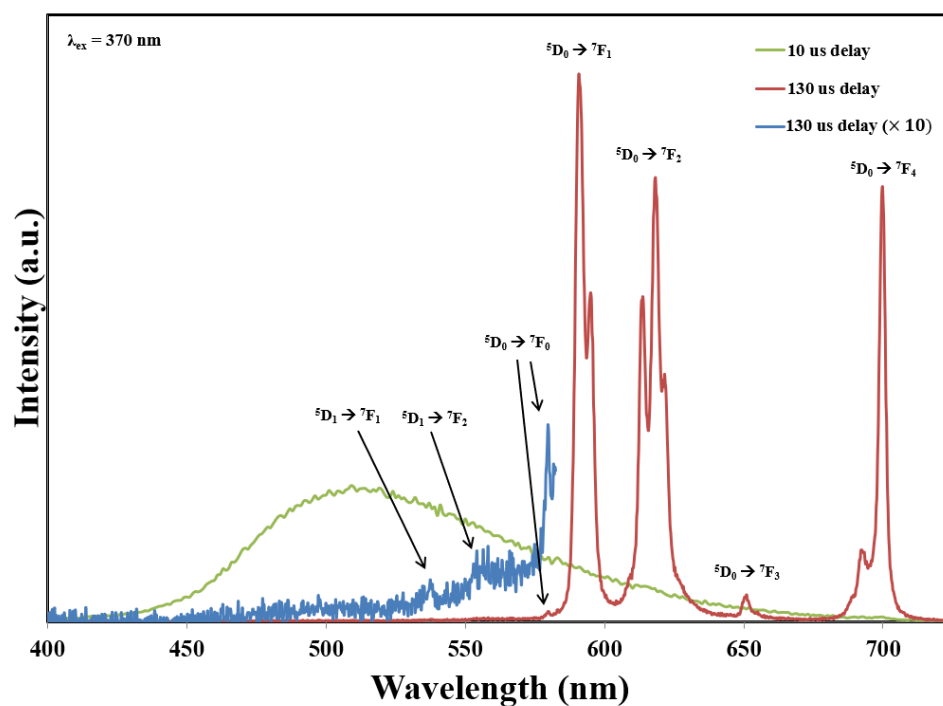

Figure 4. Room temperature, gated emission spectra collected with 370 nm excitation and 10 or 130 μs time delays.
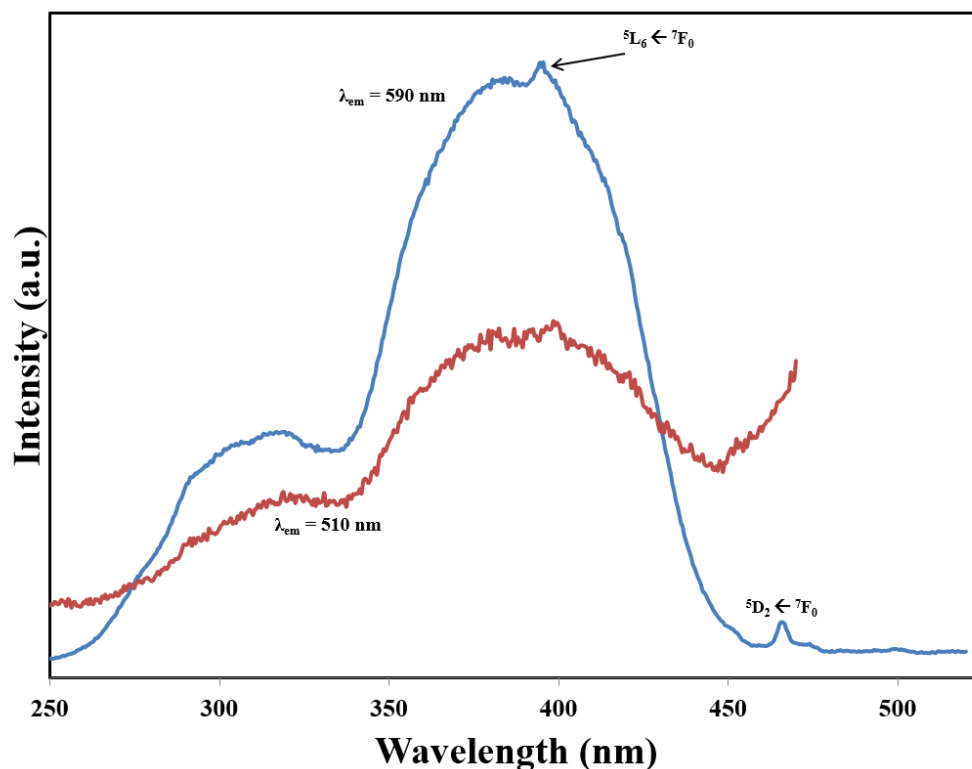
Figure 5. Room temperature, solid-state excitation spectra collected at 510 and 590 nm emission. The excitation spectrum monitored at the 590 nm emission is provided at a one-tenth scale.

4. Conclusions

Structural and spectroscopic features of $Eu_2(Pt(CN)_4)_3(H_2O)_{12}\cdot4C_{11}H_6N_2O\cdot6H_2O)$, a new member of the lanthanide tetracyanoplatinate family, are presented. The structural analyses reveal that this compound contains a molecular structure with $[Eu_2(Pt(CN)_4)_3(H_2O)_{12}]$ molecules in which the Eu^{3+} sites are connected with trans-bridging $[Pt(CN)4]^{2-}$ anions. The structure is stabilized by multiple intermolecular interactions, including H-bonding and stacking interactions involving the square planar tetracyanoplatinate anions and dafone molecules. The solid-state photoluminescence characterization illustrates that multiple emitting states are present for $Eu_2(Pt(CN)_4)_3(H_2O)_{12}\cdot4C_{11}H_6N_2O\cdot6H_2O$, and the compound also displays enhanced Eu^{3+}-based emission as a result of energy transfer within the compound.

References

1. Chorazy, S.; Wyczesany, M.; Sieklucka, B. Lanthanide Photoluminescence in Heterometallic Polycyanidometallate-Based Coordination Networks. *Molecules* **2017**, *22*, 1902. [CrossRef] [PubMed]
2. Ferbinteanu, M.; Cimpoesu, F.; Tanase, S. Metal-Organic Frameworks with d-f Cyanide Bridges: Structural Diversity, Bonding Regime, and Magnetism. *Struct. Bond.* **2014**, *163*, 185–229.
3. Rocha, J.; Carlos, L.D.; Paz, F.A.A.; Ananias, D. Luminescent multifunctional lanthanides-based metal-organic frameworks. *Chem. Soc. Rev.* **2011**, *40*, 926–940. [CrossRef] [PubMed]
4. Cairns, A.B.; Catafesta, J.; Levelut, C.; Rouquette, J.; van der Lee, A.; Thompson, A.L.; Dmitriev, V.; Haines, J.; Goodwin, A.L. Giant negative linear compressibility in zinc dicyanoaurate. *Nat. Mater.* **2013**, *12*, 212–216. [CrossRef]
5. Akitsu, T.; Einaga, Y. Structures, magnetic properties, and XPS of cyanide-bridged NdIII/SmIII/GdIII–CrIII complexes. *Inorg. Chim. Acta* **2006**, *359*, 1421–1426. [CrossRef]
6. Pal, S.; Jagadeesan, D.; Gurunatha, K.; Eswaramoorthy, M.; Maji, T. Construction of bi-functional inorganic-organic hybrid nanocomposites. *J. Mater. Chem.* **2008**, *18*, 5448–5451. [CrossRef]
7. Li, G.; Akitsu, T.; Sato, O.; Einaga, Y. Three-dimensional 3d–4f hetero-bimetallic coordination polymers through hydrogen bonds: Synthesis, structures and mössbauer spectrum analysis. *J. Coord. Chem.* **2004**, *57*, 855–864. [CrossRef]
8. Assefa, Z.; Shankle, G.; Patterson, H.H.; Reynolds, R. Photoluminescence studies of lanthanide ion complexes of gold and silver dicyanides: A new low-dimensional solid state class for nonradiative excited-state energy transfer. *Inorg. Chem.* **1994**, *33*, 2187–2195. [CrossRef]
9. Rawashdeh-Omary, M.A.; Omary, M.A.; Shankle, G.E.; Patterson, H.H. Luminescence Thermochromism in Dicyanoargentate(I) Ions Doped in Alkali Halide Crystals. *J. Phys. Chem. B* **2000**, *104*, 6143–6151. [CrossRef]
10. Gliemann, G.; Yersin, H. Spectroscopic Properties of the Quasi One-Dimensional Tetracyanoplatinate(II) Compounds. *Struct. Bond.* **1985**, *62*, 87–153.
11. Arthur, R.B.; Nicholas, A.D.; Roberts, R.J.; Assefa, Z.; Leznoff, D.B.; Patterson, H.H. Luminescence Investigation of Samarium(III)/Dicyanoaurate(I)-based Coordination Networks with and without Aurophilic Interactions. *Gold Bull.* **2018**, *51*, 1–10. [CrossRef]
12. Roberts, R.J.; Le, D.; Leznoff, D.B. Color-Tunable and White-Light Luminescence in Lanthanide Dicyanoaurate Coordination Polymers. *Inorg. Chem.* **2017**, *56*, 7948–7959. [CrossRef] [PubMed]
13. Tanner, P.A.; Zhou, X.; Wong, W.-T.; Kratzer, C.; Yersin, H. Structure and Spectroscopy of Tb[Au(CN)$_2$]$_3$·3H$_2$O. *J. Phys. Chem. B* **2005**, *109*, 13083–13090. [CrossRef] [PubMed]
14. Shore, S.G.; Ding, E.; Park, C.; Keane, M.A. The application of {(DMF)$_{10}$Yb$_2$[TM(CN)$_4$]$_3$}$_\infty$ (TM = Ni, Pd) supported on silica to promote gas phase phenol hydrogenation. *J. Mol. Catal. A Chem.* **2004**, *212*, 291–300. [CrossRef]
15. Rath, A.; Aceves, E.; Mitome, J.; Liua, J.; Ozkanb, U.S.; Shore, S.G. Application of {(DMF)$_{10}$Ln$_2$[Pd(CN)$_4$]$_3$}$_\infty$ (Ln = Yb, Sm) as lanthanide-palladium catalyst precursors dispersed on sol-gel-TiO$_2$ in the reduction of NO by methane in the presence of oxygen. *J. Mol. Catal. A Chem.* **2001**, *165*, 103–111. [CrossRef]
16. Leznoff, D.B.; Xue, B.-Y.; Batchelor, R.J.; Einstein, F.W.B.; Patrick, B.O. Gold−Gold Interactions as Crystal Engineering Design Elements in Heterobimetallic Coordination Polymers. *Inorg. Chem.* **2001**, *40*, 6026–6034. [CrossRef]
17. Fernández, E.J.; Laguna, A.; López-de-Luzuriaga, J.M. Gold-heterometal complexes. Evolution of a new class of luminescent materials. *Dalton Trans.* **2007**, 1969–1981. [CrossRef]
18. Holzapfel, W.; Yersin, H.; Gliemann, G. The structures of the tetracyanoplatinates, a class of quasi-one dimensional systems. *Z. Kristallograp.* **1981**, *157*, 47–67. [CrossRef]
19. Neuhausen, C.; Pattison, P.; Schiltz, M. A new polymorph of dicesium tetracyanoplatinate monohydrate with unusual platinum stacking. *CrystEngComm* **2011**, *13*, 430–432. [CrossRef]
20. Bünzli, J.-C.G. Lanthanide Luminescence for Biomedical Analyses and Imaging. *Chem. Rev.* **2010**, *110*, 2729–2755. [CrossRef]
21. Vuojola, J.; Soukka, T. Luminescent lanthanide reporters: New concepts for use in bioanalytical applications. *Methods Appl. Fluoresc.* **2014**, *2*, 012001. [CrossRef] [PubMed]
22. Monteiro, J.H.S.K. Recent Advances in Luminescence Imaging of Biological Systems Using Lanthanide(III) Luminescent Complexes. *Molecules* **2020**, *25*, 2089. [CrossRef] [PubMed]
23. Nampi, P.P.; Vakurov, A.; Mackenzie, L.E.; Scrutton, N.S.; Millner, P.A.; Jose, G.; Saha, S. Selective cellular imaging with lanthanide-based upconversion nanoparticles. *J. Biophotonics* **2019**, *12*, e201800256. [CrossRef] [PubMed]
24. Kuriki, K.; Koike, Y.; Okamoto, Y. Plastic Optical Fiber Lasers and Amplifiers Containing Lanthanide Complexes. *Chem. Rev.* **2002**, *102*, 2347–2356. [CrossRef] [PubMed]
25. Bünzli, J.-C.G.; Piguet, C. Taking advantage of luminescent lanthanide ions. *Chem. Soc. Rev.* **2005**, *34*, 1048–1077. [CrossRef] [PubMed]
26. Moore, E.G.; Samuel, A.P.S.; Raymond, K.N. From Antenna to Assay: Lessons Learned in Lanthanide Luminescence. *Acc. Chem. Res.* **2009**, *42*, 542–552. [CrossRef]
27. De Bettencourt-Dias, A.; Rossini, J.S.K. Ligand Design for Luminescent Lanthanide-Containing Metallopolymers. *Inorg. Chem.* **2016**, *55*, 9954–9963. [CrossRef]

28. Molloy, J.K.; Lincheneau, C.; Karimdjy, M.M.; Agnese, F.; Mattera, L.; Gateau, C.; Reiss, P.; Imbert, D.; Mazzanti, M. Sensitisation of visible and NIR lanthanide emission by INPZnS quantum dots in bi-luminescent hybrids. *Chem. Commun.* **2016**, *52*, 4577–4580. [CrossRef]

29. Chandra, A.; Singh, K.; Singh, S.; Sivakumar, S.; Patra, A.K. A luminescent europium(III)-platinum(II) heterometallic complex as a theranostic agent: A proof-of-concept study. *Dalton Trans.* **2016**, *45*, 494–497. [CrossRef]

30. Dang, S.; Yu, J.-B.; Wang, X.-F.; Guo, Z.-Y.; Sun, L.-N.; Deng, R.-P.; Feng, J.; Fan, W.-Q.; Zhang, H.-J. A study on the NIR-luminescence emitted from ternary lanthanide [Er(III), Nd(III) and Yb(III)] complexes containing fluorinated-ligand and 4,5-diazafluroen-9-one. *J. Photochem. Photobio. A Chem.* **2010**, *214*, 152–160. [CrossRef]

31. Maynard, B.A.; Smith, P.A.; Ladner, L.; Jaleel, A.; Beedoe, N.; Crawford, C.; Assefa, Z.; Sykora, R.E. Emission enhancement through Dual Donor Sensitization: Modulation of Structural and Spectroscopic Properties in a Series of Europium Tetracyanoplatinates. *Inorg. Chem.* **2009**, *48*, 6425–6435. [CrossRef] [PubMed]

32. Maynard, B.A.; Kalachnikova, K.; Whitehead, K.; Assefa, Z.; Sykora, R.E. Intramolecular Energy Transfer in a One-Dimensional Europium Tetracyanoplatinate. *Inorg. Chem.* **2008**, *47*, 1895–1897. [CrossRef] [PubMed]

33. Ladner, L.; Ngo, T.; Crawford, C.; Assefa, Z.; Sykora, R.E. Solid-State Photoluminescence of Tb^{3+} by Novel Au_2Pt_2 and Au_2Pt_4 Cyanide Clusters. *Inorg. Chem.* **2011**, *50*, 2199–2206. [CrossRef] [PubMed]

34. Hendrich, J.M.; White, F.D.; Sykora, R.E. Lanthanide dicyanoaurate coordination polymers containing 1,10-phenanthroline: Synthesis, structure, and luminescence. *Inorg. Chim. Acta* **2021**, *527*, 120562. [CrossRef]

35. Smith, P.A.; Crawford, C.; Beedoe, N.; Assefa, Z.; Sykora, R.E. Synthesis, Crystal Structures, and Dual Donor Luminescence Sensitization in Novel Terbium Tetracyanoplatinates. *Inorg. Chem.* **2012**, *51*, 12230–12241. [CrossRef]

36. Gabbaï, F.P.; Chirik, P.J.; Fogg, D.E.; Meyer, K.; Mindiola, D.J.; Schafer, L.L.; You, S.-L. An Editorial About Elemental Analysis. *Organometallics* **2016**, *35*, 3255–3256. [CrossRef]

37. Robinson, N.J.; Smith, P.A.; Grant, S.; Whitehead, K.; Crawford, C.; Assefa, Z.; Sykora, R.E. Novel tetracyanoplatinates with the larger Ln^{3+} ions: Synthesis, structures, and photoluminescence properties of K*Ln*[Pt(CN)$_4$]$_2$·8.75H$_2$O (*Ln* = La, Pr, Nd). *Inorg. Chim. Acta* **2013**, *394*, 459–465. [CrossRef]

38. Agilent. *CrysAlis PRO*; Agilent Technologies Ltd.: Oxfordshire, UK, 2013.

39. Sheldrick, G.M. Crystal structure refinement with. *SHELXL Acta Cryst. Sec. C* **2015**, *71*, 3–8.

40. Stojanovic, M.; Robinson, N.J.; Chen, X.; Sykora, R.E. Reduction of structural dimensionality through incorporation of auxiliary ligands in lanthanide tetracyanoplatinates. *Inorg. Chim. Acta* **2011**, *370*, 513–518. [CrossRef]

41. Sredojevic, D.N.; Tomic, Z.D.; Zaric, S.D. Influence of metal and ligand types on stacking interactions of phenyl rings with square-planar transition metal complexes. *Cen. Eur. J. Chem.* **2007**, *5*, 20–31. [CrossRef]

42. Qian, D.-J.; Leng, W.-N.; Zhang, Y.; Chen, Z.; Van Houten, J. A study of the fluorescence of some newly synthesized europium complexes with pyrazolone derivatives. *Spectrochim. Acta Part A* **2000**, *56*, 2645–2651. [CrossRef] [PubMed]

43. Horrocks, W.D., Jr.; Sudnick, D.R. Lanthanide Ion Luminescence Probes of the Structure of Biological Macromolecules. *Acc. Chem. Res.* **1981**, *14*, 384–392. [CrossRef]

44. Puntus, L.; Zhuravlev, K.; Lyssenko, K.; Antipin, M.; Pekareva, I. Luminescence and structural properties of lanthanide complexes of Schiff bases derived from pyridoxal and amino acids. *Dalton Trans.* **2007**, 4079–4088. [CrossRef] [PubMed]